Modeling the Impact of Wi-Fi 6E Traffic on Ultra-Wideband Communication Performance

Michael Stocker
Graz University of Technology
Graz, Austria
michael.stocker@tugraz.at

Alexander Bögl
Graz University of Technology
Graz, Austria
alexander.boegl@student.tugraz.at

Elisei Ember
Pro2Future GmbH
Graz, Austria
elisei.ember@hotmail.com

Maximilian Schuh
Graz University of Technology
Graz, Austria
schuh@tugraz.at

Kay Römer
Graz University of Technology
Graz, Austria
roemer@tugraz.at

Carlo Alberto Boano
Graz University of Technology
Graz, Austria
cboano@tugraz.at

Stefan Tertinek
NXP Semiconductors
Gratkorn, Austria
stefan.tertinek@nxp.com

Pablo Corbalán Pelegrín
NXP Semiconductors
Gratkorn, Austria
pablo.corbalan@ieee.org

***Abstract*—The growing proliferation of Wi-Fi 6E devices, which operate at a high transmission power in the same frequency band used by ultra-wideband (UWB) technology, poses significant challenges to the reliability of UWB-based systems. Prior work has explored the impact of Wi-Fi 6E traffic on UWB performance *experimentally* using real-world testbeds, but lacks a *theoretical framework* capturing how Wi-Fi 6E's physical-layer (PHY) settings, signal strength, and traffic profile affect UWB performance. We address this gap by introducing a probabilistic error model that accurately estimates the packet error rate (PER) of UWB systems operating alongside Wi-Fi 6E traffic. Using a conducted test setup, we analyze coexisting transmissions to characterize real-world Wi-Fi 6E traffic (e.g., airtime, inter-arrival times, and channel occupancy) and quantify the sensitivity of UWB transmissions to Wi-Fi 6E interference for different PHY settings, traffic profiles, and signal strengths. We leverage this characterization to parametrize the model using different approaches, ranging from a trace-based estimation of the collision probability to an analytical derivation of Wi-Fi 6E's channel occupancy. This allows us to explore different trade-offs w.r.t. the model's accuracy and generality. Our experimental evaluation demonstrates that our model accurately captures the UWB PER, with average deviations as low as 3.6% on conducted measurements and below 9.7% on real-world experiments in a university building.**

***Index Terms*—Coexistence, Interference, PER, SIR, UWB.**

I. Introduction

Ultra-wideband (UWB) has emerged as one of the most popular low-power wireless technologies for designing location-aware IoT applications. UWB radios offer indeed a unique combination of fine time resolution, multipath resilience, and low power consumption, which enables the development of cm-accurate positioning systems across application domains as diverse as robot localization [1], occupancy sensing in vehicles [2], and tracking of visitors in caves [3] or museums [4]. Whilst the use of a high bandwidth enables the transmission of very short signal pulses (≈ 2 ns long) – which allows UWB radios to precisely measure the time-of-arrival (ToA) of a frame and, consequently, to accurately estimate the distance between devices – it also introduces several challenges.

In fact, to minimize interference with co-located narrowband systems, regulatory bodies impose limits on the maximum transmission power of UWB signals, which is ≈ 14–50 dB lower than that of common narrowband technologies such as Bluetooth and Wi-Fi. As a consequence, UWB transmissions are highly vulnerable to those of nearby wireless devices operating at higher power on the same frequencies. UWB's low signal energy (and carrier-less nature) further complicates energy detection: as a result, UWB radios lack clear channel assessment capabilities and cannot implement carrier sense multiple access (CSMA) to avoid collisions [5]. Moreover, standard interference mitigation techniques such as channel blacklisting or frequency diversity are not viable due to the limited number of available UWB channels [6].

Coexistence between UWB and Wi-Fi. UWB's limited ability to coexist with other wireless technologies has become *critical* with the release of the IEEE 802.11ax (Wi-Fi 6E) and IEEE 802.11be (Wi-Fi 7) standards, which expand the operational frequencies of Wi-Fi into the 6 GHz band. In fact, UWB channel 5 also falls within this band, and is among the few UWB channels recommended to ensure global compatibility and interoperability across platforms.

Recent studies [7], [8], [9], [10], [11] have shown experimentally that Wi-Fi 6E traffic may completely disrupt UWB communications on channel 5. This results in significant degradation of ranging and localization performance, with UWB-based systems achieving success rates as low as 4% in completing two-way ranging amid Wi-Fi 6E traffic [7].

While these studies laid the groundwork for understanding (and mitigating) the impact of Wi-Fi 6E traffic on co-located UWB systems, their primary goal was to empirically *show and quantify the extent* of the coexistence problem through real-world experiments, rather than to *develop a general model* capable of predicting UWB's communication performance in the presence of Wi-Fi 6E interference. Such a model would support the design of reliable UWB-based systems, allow their deployment in crowded wireless environments, reduce the need for extensive empirical testing, and enable integration into network simulators such as OMNET++ or ns3.

Lack of suitable models. To the best of our knowledge, there is no such model in the literature. Existing works investigating on a theoretical basis the UWB performance under additive white gaussian noise (AWGN) or narrowband interference

mainly date back to more than a decade ago [12], [13], [14], [15] – to a time when no off-the-shelf UWB radios compliant to the IEEE 802.15.4 standard were yet available – or focus on ranging and ToA estimation rather than communication [16], [17], [18]. Although providing useful insights, these models hence do not capture the communication performance of (nor were validated on) real-world UWB devices. Besides that, these works do not consider Wi-Fi's PHY settings and timing characteristics, both of which are crucial for accurate error prediction. Models considering the temporal alignment of Wi-Fi packets and other coexisting wireless transmissions exist in the literature. One example is the probabilistic model of Bluetooth's packet error rate (PER) in the presence of Wi-Fi interference devised by Shellhammer [19]. Although this model captures the alignment of Wi-Fi and Bluetooth frames on the air, as well as the sensitivity of Bluetooth's modulation scheme to predict packet errors [20], it is specifically tailored to Bluetooth (which uses a single modulation scheme) and to IEEE 802.11n (i.e., Wi-Fi 4 – which operates in the 2.4 and 5 GHz bands with a bandwidth up to 40 MHz). In contrast, Wi-Fi 6E shares the 6 GHz band with UWB devices (which employ different modulation schemes to transmit a frame's preamble and payload), and can use bandwidths up to 160 MHz. Other models available in the literature also suffer similar limitations: as a result, to date, there is no usable model allowing us to predict the UWB PER in the presence of traffic generated by devices compliant to the latest Wi-Fi standards.

Contributions. We fill this gap by introducing a probabilistic model inspired by [19] that can accurately estimate the PER of UWB-based systems operating alongside Wi-Fi 6E traffic.

To this end, using a *conducted measurement setup*, we first analyze coexisting UWB and Wi-Fi 6E traffic. This allows us to *characterize* real-world Wi-Fi 6E traffic (deriving channel occupancy as well as airtime and inter-arrival time of packets), and to capture the sensitivity of UWB transmissions to Wi-Fi 6E traffic for different PHY settings (e.g., bandwidth and channel center frequency), data rates, and signal strengths.

We use the outcome of this characterization to *parametrize* the aforementioned model, i.e., we derive scaling and shaping parameters from the conducted measurements for accurate packet error rate modeling. We adopt multiple parametrization approaches, ranging from extracting the probability of frame collision directly from real-world traces of coexisting Wi-Fi 6E and UWB traffic to analytically deriving the Wi-Fi 6E's channel occupancy based on a description of its PHY settings and traffic profile. This allows us to explore different trade-offs w.r.t. the model's accuracy and generality.

We first evaluate our model using traces from the conducted test setup, showing that the most accurate parametrization approach deviates by only 3.6% on average from the actual PER of UWB transmissions. We finally validate our model through real-world experiments in which UWB and Wi-Fi 6E devices are co-located in a university building. Our results demonstrate that our model accurately captures the PER of UWB transmissions in the presence of different types of Wi-Fi 6E traffic, with an average error below 9.7%.

Paper outline. After introducing UWB, Wi-Fi 6E, and related work (§ II), this paper proceeds as follows:

- We present a probabilistic model that captures the UWB PER in the presence of Wi-Fi 6E traffic (§ III);
- We parametrize the model, exploring different trade-offs w.r.t. the model's accuracy and generality (§ IV);
- We evaluate our model's accuracy experimentally (§ V);
- We finally conclude the paper (§ VII) after discussing open challenges and future work (§ VI).

II. Background and Related Work

This section outlines first key aspects of UWB technology (§ II-A) and Wi-Fi 6E (§ II-B). It then reviews existing works that focus on their coexistence and that model their operation or performance in the presence of co-located traffic (§ II-C).

A. Overview of the IEEE 802.15.4 UWB PHY

UWB support for low-rate WPANs was first published in the IEEE 802.15.4a amendment in 2007 and finally merged into the IEEE 802.15.4 standard in 2011 [21]. The standardization process triggered the creation of low-cost UWB transceivers, with the Decawave DW1000 – launched in 2013 – being one of the first chipsets to be widely used for academic research and industrial prototyping. Over the past decade, a growing number of UWB transceivers from various vendors have entered the market, becoming increasingly pervasive in smartphones and modern vehicles. At the same time, support for the UWB PHY has evolved into the IEEE 802.15.4z/ab standard, which offers enhanced security, robustness, and data rates to enable a broader range of precise and secure ranging applications [22].

UWB frame structure. An IEEE 802.15.4-compliant UWB frame consists of a *synchronization header* (SHR), which enables frame detection and fine-grained ToA estimation, as well as a *data portion* [21]. These two frame portions are sent using *different modulation schemes*: the SHR uses single-pulse modulation, whereas the data portion is sent using a combination of burst position modulation and binary phase-shift keying (BPM/BPSK). The SHR consists of multiple *preamble* symbols, i.e., a sequence of ≈ 2 ns-long pulses drawn from a ternary alphabet $\{-1, 0, 1\}$ called preamble code, and a *start of frame delimiter* – consisting also of preamble symbols – that identifies the beginning of the data portion. The number of preamble symbol repetitions (PSR), typically 32 or 64, increases the signal-to-noise ratio (SNR) by averaging repeated symbols, thereby enhancing detection reliability even in the presence of noise or interference. This makes the SHR the most resilient segment of an UWB frame and the last to be affected by low SNR [8], [23]. The data portion consists of a physical header (PHR) and a payload (a.k.a. PSDU) carrying up to 127 bytes of data. Integrity of the data portion is ensured through a cyclic redundancy check and a forward error correction scheme. The payload can be sent at a data rate of 110 kbit/s, 850 kbit/s, 6.8 Mbit/s. The PHR is sent at 850 kbit/s by default or at 110 kbit/s when also the payload is transmitted at this rate.

To enable a secure ToA estimation, the IEEE 802.15.4z standard introduces the scrambled timestamp sequence (STS), a pseudo-random sequence of pulses derived from a shared secret between sender and receiver. The STS can be placed at different positions within an UWB frame; in this paper, we implicitly refer to the `SP0` configuration where the STS is omitted, as it ensures interoperability with IEEE 802.15.4a.

UWB transmission power and emission limits. To prevent interference with other co-located systems, the wideband nature of UWB is subject to strict emission limits on the average power spectral density (PSD) (-41 dBm/MHz) and effective isotropic radiated power (EIRP) (-14 dBm) over a 1 ms period. In practice, this means that shorter UWB transmissions can use a higher transmission power while still complying with the average power limits. As a result of these low power constraints, UWB receivers must achieve a high sensitivity to reliably process incoming packets: in BPRF mode at 6.81 Mbps, sensitivities as low as -94 to -97 dBm are typically required, which is ≈ 10 dB below the thermal noise floor of a 500 MHz wide channel. In practical environments, UWB receivers may be subject to narrowband interference, which raises the noise floor non-uniformly across the band.

B. A Primer on Wi-Fi 6E

Wi-Fi is one of the most ubiquitous wireless communication technologies, providing high-speed connectivity for billions of devices across homes, enterprises, and public spaces. Since its introduction in the late 1990's, the standard has undergone multiple revisions to meet growing demands for faster and more reliable wireless connectivity – most notably with Wi-Fi 6E (IEEE 802.11ax [24]) and the more recent Wi-Fi 7 (IEEE 802.11be [25]). Especially Wi-Fi 6E represents a key milestone in the history of Wi-Fi, as it introduces support for the 6 GHz frequency band. This additional spectrum capacity enables additional channels with larger bandwidths, improving overall network performance [26], [27].

Similar to UWB, the PSD of Wi-Fi 6E transmissions is regulated [24] to optimize spectral efficiency while minimizing interference with other technologies operating in the 6 GHz band. Regulatory bodies define different classes of Access Points (APs), each with specific power and spectrum usage constraints. Standard-Power (SP) APs are permitted to transmit with an EIRP of up to 36 dBm or a maximum PSD of 23 dBm/MHz. These APs are intended for both indoor and outdoor deployments, but are restricted from operating across the full 6 GHz band. In contrast, Low Power Indoor (LPI) APs are allowed to access the entire 6 GHz spectrum, but are limited to a maximum EIRP of 30 dBm or a PSD of 5 dBm/MHz, which restricts their range to mitigate cross-device interference. Very Low Power (VLP) APs are further constrained, with a maximum EIRP of 14 dBm or a PSD of -8 dBm/MHz, and are designed for short-range applications in both indoor and outdoor settings. Client devices associated with either SP or LPI access points are required to transmit at power levels 6 dB lower than the respective APs, promoting fair and efficient spectrum utilization across the network [28].

C. Related Work

We review next prior work on UWB coexistence with Wi-Fi 6E as well as other narrowband technologies, and on modeling the effects of interference caused by Wi-Fi traffic.

Performance of UWB under interference. The first works studying the performance and robustness of UWB systems under interference date back to the early to mid-2000s, in conjunction with the prospect of an UWB PHY being standardized as part of IEEE 802.15.3 or IEEE 802.15.4. Works such as [13], [14], [15] have evaluated the performance of various pulse-modulations and error correction schemes through simulations under additive white Gaussian noise and single-tone narrowband interferers. Ahmadian et al. [12] later focused on the modulation and error correction schemes foreseen in the IEEE 802.15.4a standard, and derived a semi-analytical evaluation framework for studying the bit- and frame-error rate. However, because these studies preceded both the formalization of the standard and the commercialization of the first UWB radios, they have not been validated on actual devices, which limits their practical value. More recent works have studied the performance across co-located UWB systems [29] and the coexistence between UWB and 5G [30], [31].

Coexistence of UWB and Wi-Fi 6E. The opening of the 6 GHz unlicensed band for Wi-Fi use has prompted a growing number of empirical studies investigating the coexistence between Wi-Fi 6E and UWB systems. These studies consistently show how the presence of Wi-Fi 6E traffic can cause substantial degradation in UWB performance, affecting both the reliability of communications and the accuracy/precision of ranging measurements. Brunner et al. [7] were the first to experimentally quantify the extent of UWB performance degradation using a testbed facility consisting of 36 Qorvo DW1000 devices and five Qualcomm QCN9074 Wi-Fi 6E modules. Their results were confirmed by testbed experiments performed with newer-generation UWB radios [8], [9]. Other studies have also touched upon the impact of Wi-Fi 6E or International Mobile Telecommunication (IMT) transmitters on UWB sensitivity [10], ranging success rate [11], and ToA estimation [16], [17], [18]. While all these studies help understanding the practical impact that coexisting traffic has on UWB systems, they do not provide a way to *model* or estimate the PER of UWB-based systems operating alongside Wi-Fi 6E traffic, which is the goal of this work.

Modeling the impact of Wi-Fi interference. Numerous researchers have modeled the coexistence of Wi-Fi and other narrowband wireless technologies, especially Bluetooth and IEEE 802.15.4 (or its derivatives, such as TSCH [32] and ZigBee [33]). For example, Yuan et al. [34] model the coexistence between IEEE 802.15.4 and IEEE 802.11b/g networks as a function of signal power levels and typical packet timings under various CSMA/CA scenarios. Shellhammer et al. [19], [20] propose instead a probabilistic framework to model the PER of Bluetooth as a function of the signal-to-interference ratio (SIR) and packet timings of Wi-Fi traffic. Unfortunately, these and many other works examine older versions of Wi-Fi

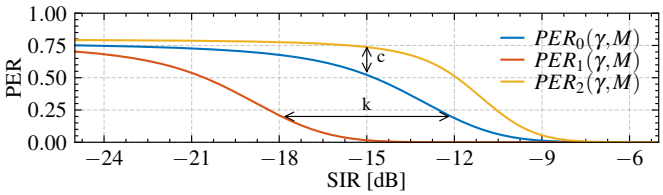

Fig. 1: Simulated PER curves as a function of SIR. Parameters k and c, discussed in § III-B, shift the curves left/right and influence the curve shapes / maximum values, respectively.

and primarily investigate its impact on other narrowband technologies operating in the 2.4 GHz band [35] or in LTE's unlicensed spectrum [36], [37], without addressing UWB. In contrast, in this paper, we specifically focus on the impact that Wi-Fi 6E (which operates on the 6 GHz band and employs bandwidths up to 160 MHz) has on UWB communications.

III. Proposed Model

We model the UWB packet error rate (PER) in the presence of Wi-Fi 6E traffic by applying the law of total probability, building on the methodology proposed in [19]:

$$PER(\gamma, M) = \sum_{m=0}^{M} P(PE|\gamma, m) f(m) \tag{1}$$

Here, M denotes the number of symbols in a UWB frame, where each symbol corresponds to a fixed 1 μs segment of the frame[1]. $P(PE|\gamma, m)$ is the probability of a packet error (PE) given that m symbols are interfered at a certain signal-to-interference ratio (SIR) γ in dB. $f(m)$ is the probability that exactly m symbols are interfered. Fig. 1 illustrates sample PER curves for varying $P(PE|\gamma, m)$ values as a function of the SIR, showing different PER growth under low-SIR conditions. We discuss next how to calculate $f(m)$ (§ III-A) and how to parameterize $P(PE|\gamma, m)$ (§ III-B). We derive both $f(m)$ and the parameters of $P(PE|\gamma, m)$ from conducted measurements on real-world UWB and Wi-Fi 6E devices. We then also investigate approaches to estimate $f(m)$ that do not require detailed real-world traces, but only high-level information about the frame length and inter-arrival time, as well as the Wi-Fi 6E channel occupancy. This allows us to explore different trade-offs w.r.t. the model's accuracy and generality.

A. The Symbol Collision Distribution (SCD)

The first component in our interference modeling framework is the Symbol Collision Distribution (SCD), denoted as $f(m)$ in Eq. 1. This probability mass function represents the likelihood that exactly m symbols overlap with (or "are hit by") Wi-Fi 6E transmissions, i.e., it captures the temporal interplay between Wi-Fi 6E and UWB traffic. We estimate the corresponding SCD using four different approaches, which are detailed next.

Exhaustive Sweep (ES). This approach directly extracts the SCD from real-world traces by overlaying UWB frames on top of recorded Wi-Fi 6E traffic at different time offsets. Fig. 2(a) shows a portion of a sample trace recorded using our conducted measurement setup (detailed in § IV-A) containing Wi-Fi 6E traffic (blue), and an overlaid 117 μs-long UWB frame transporting a 20-byte data payload (orange). We derive the number of interfered UWB symbols m as the overlap in μs between the Wi-Fi 6E and UWB frames, and estimate the corresponding SCD after sweeping the UWB frame across the entire trace with 1 μs-steps.

[1]The use of fixed 1 μs segments as symbols allows us to decouple the modeling from the underlying modulation scheme, and enables a consistent analysis of interference across the whole UWB frame. Please note that this choice is compelling, as the duration of an UWB preamble symbol and a byte of UWB data when using a data rate of 6.8 Mbps is indeed roughly 1 μs.

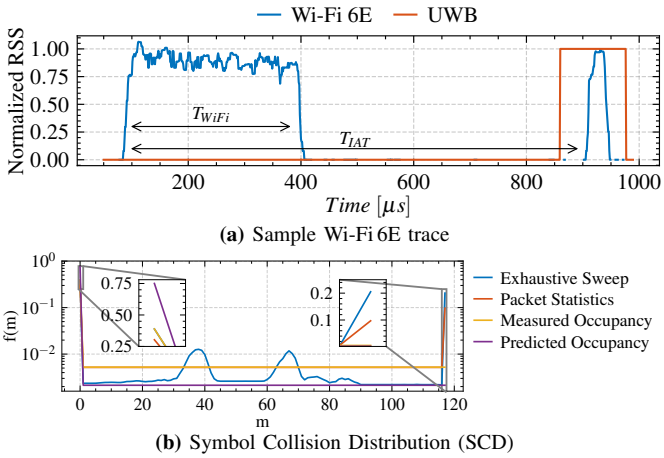

(a) Sample Wi-Fi 6E trace

(b) Symbol Collision Distribution (SCD)

Fig. 2: SCD derived from a sample real-world trace of Wi-Fi 6E traffic using four different approaches (b). This specific example refers to a trace capturing Wi-Fi 6E traffic sent using `iperf` at a rate of 200 Mbps with a 160 MHz channel bandwidth (a).

The blue curve in Fig. 2(b) shows the SCD estimated using this approach. The dominant peak at $m = 0$ reflects interference-free receptions, in which the UWB frame does not overlap with any Wi-Fi 6E activity. The second significant peak at $m = 117$ corresponds to complete overlap between UWB and Wi-Fi frames. Between these extremes lies a broad region representing partial overlaps, including smaller peaks caused by short gaps in between Wi-Fi 6E frames where the UWB frame partially fits. As a probability mass function, $f(m)$ must satisfy $\sum_{m=0}^{M} f(m) = 1$ and $f(m) \geq 0$ for all m: the entries in $f(m)$ are scaled accordingly.

Packet Statistics (PS). This approach provides an analytical approximation of the SCD based on the timings of individual Wi-Fi 6E transmissions extracted from real-world traces. Specifically, we consider three timings (the average on-air frame duration T_{WiFi}, inter-arrival time between Wi-Fi frames T_{IAT}, and UWB frame duration T_{UWB}), from which we derive:

$$\Delta T_{\text{diff}} = \left|T_{\text{UWB}} - T_{\text{WiFi}}\right|, \quad T_0 = \left|T_{IAT} - (T_{\text{WiFi}} + T_{\text{UWB}})\right|,$$
$$\text{idx}_{\text{min}} = \max\left(T_{\text{WiFi}} + T_{\text{UWB}} - T_{IAT},\, 0\right),$$
$$\text{idx}_{\text{max}} = \min\left(T_{\text{UWB}},\, T_{\text{WiFi}}\right).$$

$$f(m) = \begin{cases} \frac{T_0+1}{T_{IAT}} & m = \text{idx}_{\text{min}} \\ \frac{2}{T_{IAT}} & \text{idx}_{\text{min}} < m < \text{idx}_{\text{max}} \\ \frac{\Delta T_{\text{diff}}+1}{T_{IAT}} & m = \text{idx}_{\text{max}} \\ 0 & \text{otherwise.} \end{cases}.$$

In essence, $f(m)$ is computed by capturing four scenarios: maximum achievable overlap ($m = \text{idx}_{\text{max}}$), partial overlap

($\text{idx}_{\text{min}} < m < \text{idx}_{\text{max}}$), minimal overlap ($m = \text{idx}_{\text{min}}$), and no overlap (*otherwise*). In contrast to the ES approach – which requires detailed traces capturing the received signal strength (RSS) of Wi-Fi frames over time – only information about the timing of frames is needed.

Measured Occupancy (MO). This approach derives the Wi-Fi 6E channel occupancy o_{meas} from recorded traces. Assuming that the collision probability is uniformly distributed, we can approximate $f(m)$ as:

$$f(m) = \begin{cases} 1 - o & \text{for } m = 0 \\ o/M & \text{otherwise} \end{cases}, \quad \text{with} \quad o = o_{\text{meas}} \tag{2}$$

Predicted Occupancy (PO). In contrast to MO, this approach approximates the SCD analytically using Wi-Fi's PHY settings, making it appealing for scenarios where empirical traffic data is unavailable. We define the occupancy o_{exp} as the ratio of the anticipated and maximum possible Wi-Fi 6E data rate:

$$o = o_{\text{exp}} = \frac{DR}{DR_{max}}. \tag{3}$$

The maximum achievable data rate DR_{max} can be determined by accounting for the Wi-Fi modulation and coding scheme (MCS) as well as the number of spatial streams (NSS). Please note that both occupancy-based approaches trade accuracy for generality (no need for recorded traces), as they neither account for the UWB frame length and the temporal distribution of the Wi-Fi 6E transmissions, nor for any protocol-specific overhead (e.g., medium access control contention times). However, in practice, these methods can be used to provide a lower-bound estimation of the PER.

B. The Error Probability

Next, we discuss the conditional packet error probability ($P(PE|\gamma, m)$), which describes the likelihood of packet failure given a SIR γ and m interfered symbols in Eq. 1. Similar to [19], we adopt a standard Q-function based approximation, commonly used for characterizing bit error rates in wireless systems [38]. The error probability is modeled as:

$$P(PE|\gamma, m) = 1 - (1 - P_s(\gamma))^m \text{, with } P_s(\gamma) = cQ(\sqrt{10^{k/10}\gamma}), \tag{4}$$

where $P_s(\gamma)$ denotes the error probability of a single symbol. The parameter c scales the overall probability impacting the end-position of the curve and the curve shape, while k scales the SIR and affects the start position of the curve, as illustrated in Fig. 1. Parameters c and k can be determined empirically by fitting the modeled PER curve to the PER curves obtained through recorded traces, in contrast to [19], where they are derived analytically. We use `scipy.optimize.curve_fit` to estimate parameters by minimizing residuals between observed and modeled PERs, with the TRF method constraining c and k to $0 \leq c \leq 0.5$ and $0 \leq k \leq 25$ to avoid unrealistic values [39].

Effective interference compensation. The susceptibility of UWB systems to Wi-Fi 6E interference may not be uniform across their 500 MHz band due to filtering and other RF-specific components. To compensate for this and to derive a common value for the SIR scaling k_c, we calculate the frequency- and bandwidth-dependent loss value l_{cfbw} by numerical integration of the experimentally determined transfer-function H:

$$l_{cfbw} = 10log_{10}(\frac{1}{B}\int_{f_c-B/2}^{f_c+B/2} |H(j2\pi f)|df) \tag{5}$$

$$k = k_c - l_{cfbw} \tag{6}$$

with f_c and B the channel's center frequency and bandwidth.

C. Evaluation Metrics

To evaluate the impact of Wi-Fi 6E on UWB performance and the accuracy of our model, we define several metrics.

Hit Probability (HIP) is the probability that UWB frames overlap with Wi-Fi transmissions. Unlike traditional channel occupancy, which measures the ratio of busy to idle time, this metric directly captures the likelihood of interference at the frame level. It is computed as $\text{HIP} = 1 - f(0)$, where $f(0)$ is the probability of zero symbol collisions.

Maximum PER (MPE) is the maximum packet error rate under low-SIR conditions. While the HIP quantifies the probability of packet-symbol collisions, MPE reflects the actual resulting PER. The two may differ, for example, if symbol collisions do not consistently lead to packet errors (e.g., due to error correction mechanisms or symbol redundancy).

Packet Error Threshold (PET_x) defines the SIR at which the PER reaches threshold x. In our evaluation, we primarily use PET_{10}, which corresponds to the sensitivity specification of our UWB hardware and marks the 10% PER point.

Mean Absolute Curve Error (MAC) measures the average absolute deviation between the predicted and measured PER curves across the entire SIR range. Unlike HIP, MPE, and PET (which focus on specific operating points or regions), MAC provides a full view of the model's accuracy.

IV. Model Parametrization

This section focuses on the parametrization of the model presented in § III. We first describe our conducted measurement setup (§ IV-A). We then analyze the temporal behavior of Wi-Fi 6E traffic (§ IV-B) and its impact on the UWB PER (§ IV-C), highlighting insights relevant to our modeling effort. Building upon these measurements, we will then assess the suitability of the proposed parametrization approaches for estimating the collision probability distribution and PER (§ V).

A. Conducted Measurement Setup

Fig. 3 provides a high-level sketch of the conducted measurement setup, which consists of two Wi-Fi 6E devices and two UWB nodes interconnected through a series of power splitters/combiners and a programmable attenuator. We detail next the Wi-Fi, UWB, and measurement paths separately.

The Wi-Fi path consists of two MediaTek MT7916AN Wi-Fi 6E capable cards: one configured as access point (AP), and one as station (STA). Throughout all experiments, we set the NSS to 1 and the MCS index to 11. We then let the STA

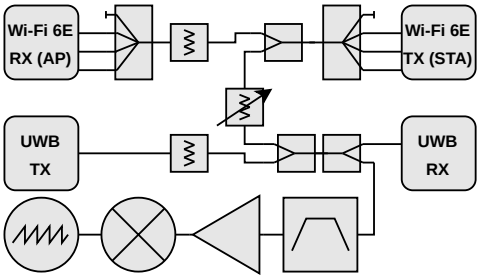

Fig. 3: The conducted measurement setup consists of two pairs of communicating Wi-Fi 6E and UWB devices. The generated Wi-Fi 6E traffic is tapped and fed to the UWB communication path through a programmable attenuator. The combined signal is tapped before it is fed to the UWB device and filtered, amplified, as well as mixed to an IF frequency of 1.5 GHz for trace generation and SIR measurements.

transmit UDP traffic on various channels utilizing the `iperf3` Linux utility[2]. In the conducted setup, the three antenna ports of each device are combined into a single communication path using 4:1 power splitters/combiners. The combined signal from the transmitting Wi-Fi 6E device is then split again using an additional 2:1 splitter/combiner. One path continues to the Wi-Fi receiver, after passing through a 6 dB attenuator that protects devices from signal overload. The second path is used to extract the Wi-Fi 6E signal for interference injection, and it is then routed into the UWB communication path via a programmable attenuator. Conversely, UWB signals may also be detected by Wi-Fi 6E devices, potentially triggering back-off events. Our setup prevents this: the use of attenuators and splitters ensures that the maximum effective received energy within a 160 MHz Wi-Fi 6E channel is limited to -96.35 dBm, which is well below the -62 dBm threshold required to trigger a back-off [24].

The UWB path consists of two UWB radios compliant to the IEEE 802.15.4z standard that are widely available on the market[3]. Both UWB nodes employ patch antennas and feature micro coaxial connectors to facilitate wired testing. Devices are enclosed in shielded metal housings to eliminate external wireless interference. To avoid overwhelming the Wi-Fi signal, the transmitted UWB signal is attenuated by 53 dB using an attenuator. This signal is then merged with the Wi-Fi signal using a power splitter/combiner and again split before being fed into the receiving UWB node to our measurement path.

The measurement path path consists of a band-pass filter in the range 5.6–7 GHz, a low-noise amplifier with 22 dB amplification, and a mixer to move Wi-Fi and UWB signals from $\approx$6.5 GHz to $\approx$1.5 GHz. This allows us to observe the UWB and Wi-Fi signals at intermediate frequency with a PlutoSDR as well as a Keysight MSO-S 254A mixed-signal oscilloscope. The former is used in zero-span mode to acquire Wi-Fi traces at a sampling rate of 1 MHz: these traces are subsequently smoothed and quantized to the interval [0,1] for further processing. The oscilloscope is primarily used to analyze both Wi-Fi and UWB frames in the frequency domain to estimate their transmission power and the relative signal strength perceived at the RX UWB device.

[2]We use `iperf` to maximize repeatability, as in related studies [7], [9].

[3]We omit hardware details, as the observed behavior reflects standard IEEE 802.15.4z protocol characteristics rather than device-specific implementations.

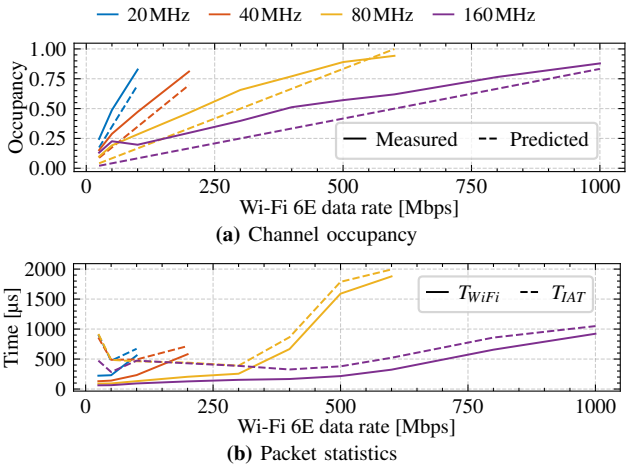

Fig. 4: Average channel occupancy (a) as well as average frame duration and inter-arrival time of Wi-Fi 6E frames (b).

B. Characterizing Wi-Fi 6E Traffic

We begin our analysis by examining the temporal characteristics of recorded Wi-Fi traffic for various data rate and channel bandwidth configurations. From these traces, we extract three key statistics: the channel occupancy, the average Wi-Fi frame duration T_{WiFi}, and the mean inter-arrival time T_{IAT}, which we use to derive the SCD (see § III-A). Fig. 4(a) shows the measured channel occupancy as a function of data rate and bandwidth, whereas Fig. 4(b) presents the corresponding values for T_{WiFi} and T_{IAT}. As expected, increasing the data rate for a given bandwidth leads to a higher channel occupancy. This relationship closely follows the approximation $o \approx DR/DR_{max}$ from Eq. 3. Moreover, doubling the bandwidth effectively halves the occupancy for the same data rate, due to the increased throughput. When analyzing the timing of individual Wi-Fi 6E transmissions, we observe that higher data rates lead to an increased T_{WiFi}, whereas T_{IAT} does not exhibit a strictly monotonic behavior. At lower data rates, T_{IAT} significantly exceeds T_{WiFi}, reflecting long idle periods between transmissions. However, once the data rate approaches approximately half of the maximum supported rate for a given bandwidth, this gap narrows. Beyond that point, the difference between T_{IAT} and T_{WiFi} stabilizes to a consistent margin of roughly 100–200 μs, indicating saturation with very small idle gaps between Wi-Fi frames.

C. Impact of Wi-Fi 6E on UWB

To quantify the impact of Wi-Fi 6E interference on UWB communication, we perform a series of controlled experiments with different traffic profiles and PHY settings. Specifically, we configure the Wi-Fi 6E devices to transmit at different data rates across various channel bandwidths and center frequencies. The UWB devices use a PSR of 64, and send SP0 frames with a PSDU length from 20 to 120 bytes. To simulate varying

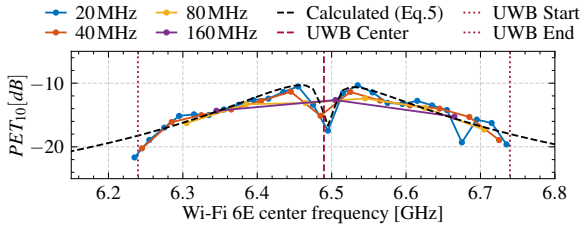

Fig. 5: PET_{10} as a function of the Wi-Fi 6E channel's center frequency and bandwidth.

interference conditions, we gradually adjust a programmable attenuator between the two UWB nodes in 1 dB steps. For each step, we transmit 1000 UWB frames and record the number of reception errors to determine the PER as a function of the SIR. For every configuration, we compute the observed PER and determine the PET_x value. These results are then compared against the output of our model, which uses the Exhaustive Sweep approach (most accurate) with parameters $c = 0.22$ and $k_c = 17.5$ as determined later in this section.

Impact of channel bandwidth and frequency. To understand the frequency sensitivity of UWB reception under Wi-Fi 6E interference, we analyze how both the bandwidth and center frequency of the Wi-Fi signal affect the PET at 10% (PET_{10}). This evaluation is motivated by the fact that the frequency response of the UWB transceiver's RF front end is non-uniform, altering the effective interference energy depending on the employed Wi-Fi channel. In this experiment, the Wi-Fi devices operate at their maximum data rate, while the UWB PSDU length is fixed at 20 bytes. We then sweep the Wi-Fi 6E channel center frequency from 6.2 GHz to 6.7 GHz, using step sizes of 20, 40, 80, and 160 MHz to match the corresponding channel bandwidths. Fig. 5 shows the resulting PET_{10} values across channel center frequencies and bandwidths. We can observe a clear frequency dependency with up to 11 dB difference in required SIR to maintain a 10% PER. In particular, the required PET_{10} tends to be lower near the edges of the 500 MHz UWB band, rises near the center frequency, and then drops again exactly at the center. This behavior can be effectively modeled by approximating the UWB front-end response as a composite filter, namely a bandpass filter spanning the 6.39–6.59 GHz range, combined with a narrow notch filter centered at 6.495 GHz with a quality factor $Q_{notch} = 300$. The black dashed curve in Fig. 5 shows the predicted PET_{10} for a 20 MHz Wi-Fi 6E channel based on this filter model, which closely matches the measured values.

Impact of Wi-Fi 6E data rate. We configure the Wi-Fi 6E devices to operate across multiple bandwidths: 20 MHz (centered at 6.495 GHz), 40 MHz (centered at 6.485 GHz), 80 MHz (centered at 6.465 GHz), and 160 MHz (centered at 6.505 GHz). Fig. 6(a) shows the measured (solid) and predicted (dashed) PER as a function of SIR for various data rates using a 160 MHz Wi-Fi channel. The results clearly show that the PER is highly affected by the data rate, particularly under low SIR conditions. This trend can be attributed to the effective channel occupancy: with increasing data rates, the occupancy rises, thereby increasing the probability of collision and packet loss.

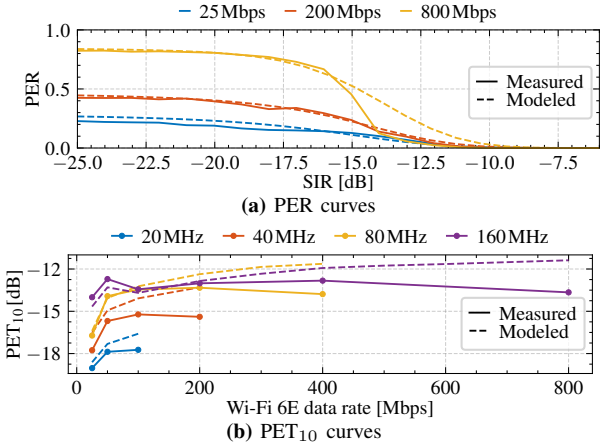

Fig. 6: Impact of Wi-Fi 6E data rates, SIR, and channel bandwidth on PER (a) and PET_{10} (b). The top plot is derived using a channel bandwidth of 160 MHz and an UWB PSDU length of 120 bytes.

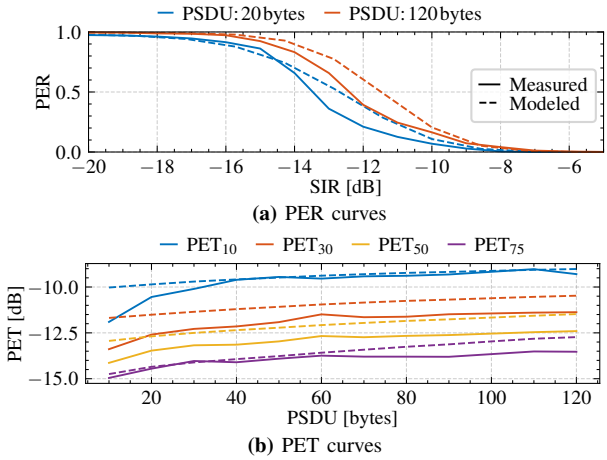

Fig. 7: Impact of UWB PSDU length on PER (a) and PET values (b). Solid lines: measured data; dashed lines: model predictions.

Depending on the chosen data rate, we observe differences in PER of up to ≈55%. In contrast, the impact of data rate on PET_{10} is less severe. As shown in Fig. 6(b), both the measured (solid) and predicted (dashed) PET_{10} exhibit a similar spread across Wi-Fi 6 data rates, ranging from 1.3 dB to 3.39 dBm for the measured, and between 2.02 dB and 4.76 dB for the predicted PET_{10}.

Impact of UWB PSDU length. We configure the Wi-Fi 6E devices to transmit on a 20 MHz-wide channel centered at 6.455 GHz with maximum available data rate, and the UWB devices to send packets with different PSDU lengths. We then record the PER while varying the SIR using a programmable attenuator. Fig. 7(a) shows that, unsurprisingly, longer data payloads are more vulnerable to Wi-Fi 6E interference, resulting in PER degradation already at lower SIR levels. Fig. 7(b) shows the corresponding PET_{10} for PSDU lengths ranging from 10 to 120 bytes. The measured data suggests up to ≈2.88 dB difference in PET_{10} as a function of packet length. This is only partially captured by the model, which predicts a higher PET_{10} value for lower PSDU lengths. This observation suggests that additional PHY effects or implementation-

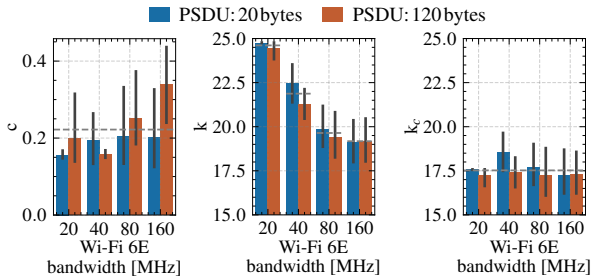

(a) Error scaling parameter c **(b)** SIR scaling parameter k **(c)** Common SIR scaling parameter k_c

Fig. 8: Error scaling parameters c and k as a function of the Wi-Fi 6E bandwidth and UWB PSDU length.

specific factors may be influencing error sensitivity beyond what our model (based on symbol collisions) accounts for.

Suitable c and k for modeling the PER. To parametrize the *error probability* $P(PE|\gamma, m)$ with suitable c and k values, we record PER curves for different Wi-Fi channel bandwidths (20 MHz, centered at 6.495 GHz; 40 MHz, centered at 6.485 GHz; 80 MHz, centered at 6.465 GHz; and 160 MHz, centered at 6.505 GHz) and data rates (between 25 and 800 Mbps), as well as UWB PSDU lengths (20 or 120 bytes). Fig. 8(a) shows the estimated parameter c across different bandwidths and PSDU lengths (averaged over all investigated data rates). For short PSDU lengths, we observe similar c values across all bandwidths and we observe a tendency for higher c values for longer PSDU lengths. This trend aligns with our expectations: the average resilience of an UWB packet improves when the relatively robust preamble and PHR outweigh the sensitivity of the data portion. As the PSDU length increases, the average packet sensitivity rises, which is reflected in a higher c value. On average, we found that $c = 0.22$ sufficiently represents all cases. The k value, shown in Fig. 8(b), determines the onset point of the curves and depends on the Wi-Fi 6E channel bandwidth and center frequency, as highlighted in Fig. 5. By applying Eq. 6, we derive the channel- and bandwidth-independent SIR scaling parameter k_c. Fig. 8(c) shows that an average value $k_c = 17.5$ sufficiently represents all measurements. During model prediction, we will use Eq. 6 to compute the channel- and bandwidth-dependent parameter k from the common k_c.

V. Evaluation

We now evaluate the accuracy of our modeling approach. First, we use the conducted measurements (§ IV-A) to assess how different parametrization approaches affect model performance. Second, we perform wireless experiments to demonstrate the applicability of the model in real-world scenarios.

A. Evaluation Using Conducted Measurements

Relationship between HIP and MPE. Under low-SIR conditions, UWB frames are highly sensitive to Wi-Fi 6E interference: even a single symbol collision can lead to a frame error. As a result, successful UWB reception typically occurs only when a frame experiences no collisions at all. Therefore, the Hit Probability (HIP), i.e., the probability of any collision,

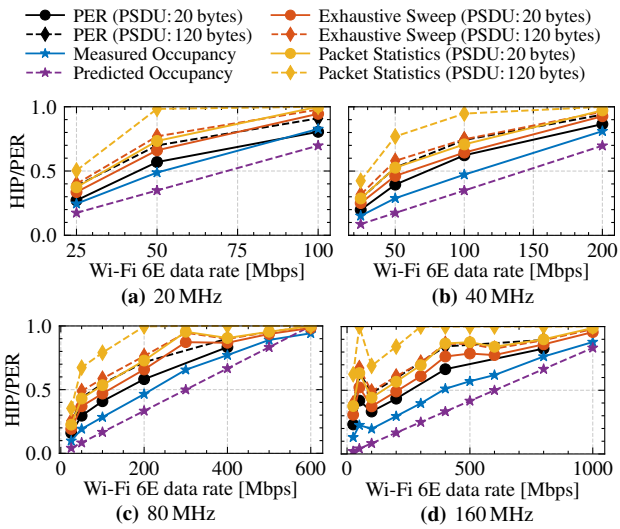

(a) 20 MHz **(b)** 40 MHz **(c)** 80 MHz **(d)** 160 MHz

Fig. 9: PER and HIP calculated with the four SCD approaches.

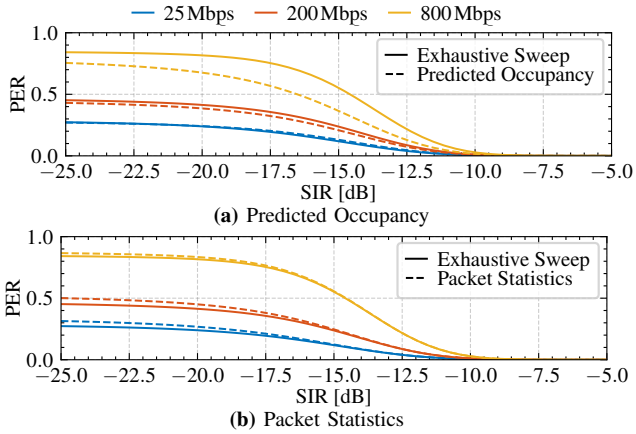

(a) Predicted Occupancy **(b)** Packet Statistics

Fig. 10: PER curve offset introduced by *occupancy* and PS methods.

directly determines the maximum PER (MPE). Fig. 9 presents the measured MPE alongside the HIP values computed using the four different SCD approximation methods introduced in § III-A. For PSDU lengths of 20 and 120 bytes, the difference between measured PER and the MPE computed using the Measured Occupancy remains within approximately -9.4% to -21.7% on average. The Predicted Occupancy method shows a $\approx 10\%$ larger offset, likely due to additional packet overhead and control frames present in Wi-Fi 6E traffic that we currently do not account for. Since this offset is stable across configurations (see Fig. 9), incorporating these overheads into the occupancy model could further improve accuracy. Using the Packet Statistics method leads to a MPE that overestimates the PER, but that achieves a lower absolute error of 12.7% and 19.3% for PSDU lengths of 20 and 120 bytes, respectively. Among all approaches, the Exhaustive Sweep is the most accurate, with differences of only 6.6% and 3.1% to the true PER for PSDU lengths of 20 and 120 bytes, respectively.

Impact of $f(m)$ on the PER shape. Next, we analyze the impact of different $f(m)$ estimation methods by comparing them against the Exhaustive Sweep approach. Fig. 10(a)

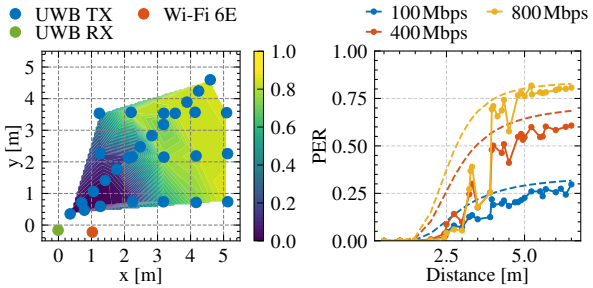

(a) PER map **(b)** PER over distance

Fig. 11: Device locations and measured PER in *office* (a). Predicted (dashed) and measured PER (solid) for various Wi-Fi 6E data-rates when using a fixed PSDU length of 20 bytes (b).

presents the PER curves obtained using Exhaustive Sweep (solid lines) and the Predicted Occupancy (dashed lines) to generate $f(m)$. We can observe two key aspects: first, when using the Predicted Occupancy approach, the end position is slightly underestimated in low SIR conditions with high Wi-Fi 6E data rates. Second, the PER curves are noticeably shallower compared to the Exhaustive Sweep approach. Both effects can be attributed to the shape of $f(m)$, which is uniform across all collision cases. In contrast, the $f(m)$ generated by the Packet Statistics method exhibits a distribution that is not uniform for all $m > 0$ and aligns much more closely with the reference curve produced via Exhaustive Sweep.

Model performance. We evaluate the final PER prediction performance of the proposed model using different SCD estimation methods. To this end, we calculate the average offset MPE, MAC, and PET_{10} between the measured and predicted PER curves. The results are shown in Tab. I: as anticipated, the Exhaustive Sweep method yields the lowest error across all three performance metrics, regardless of the UWB PSDU length. Differently, the Packet Statistics overestimate the PER by a small offset ($\approx$4.7%) in terms of MPE for short PSDUs and a high offset ($\approx$14.3%) for long PSDUs. Conversely, the occupancy-based methods underestimate the MPE value by $\approx$17.1% to $\approx$36.7%: this is also reflected by a high MAC and a negative PET_{10} value of up to -1.49 dB.

B. Wireless Evaluation

We finally evaluate the model in a wireless setup deployed in a vacant $\approx 6 \times 6$ m university *office* and a $\approx 50 \times 4$ m *hallway*. In both environments, we place the interfering Wi-Fi 6E device 1 m away from the UWB receiver, whereas the UWB transmitter is placed at various distances (as an example, the blue dots in Fig. 11(a) show the positions of the UWB transmitter in the *office*). To establish a baseline SIR, we measure the received signal strength (RSS) of both the UWB and Wi-Fi 6E devices at 1 m distance using an oscilloscope in each environment. Using these measurements, we apply the log-distance path loss model to estimate the SIR at any distance d as:

$$\text{SIR}(d) = \text{SIR}(d_0) - 10n \log_{10}(d/d_0) \quad (7)$$

$\text{SIR}(d_0)$ is the measured SIR at 1 m distance, and n is the path loss exponent. Following Molisch et al. [40], we use $n = 1.75$, which corresponds to typical residential environments. We

TABLE I: Model performance using conducted measurements.

SCD method	PSDU [bytes]	MAC [%]	MPE [%]	PET_{10} [dB]
ES	20	3.6	0.4	0.93
PS	20	5.4	4.7	0.97
MO	20	10.0	-17.1	-0.75
PO	20	16.3	-27.7	-0.98
ES	120	3.0	-0.5	-0.13
PS	120	10.1	14.3	-0.07
MO	120	17.7	-25.6	-1.41
PO	120	24.9	-36.7	-1.49

TABLE II: Model performance using wireless measurements.

SCD method	PSDU [bytes]	MAC Office [%]	MAC Hallway [%]	MPE Office [%]	MPE Hallway [%]	PET_{10} Office [dB]	PET_{10} Hallway [dB]
ES	20	6.1	9.7	4.7	4.7	2.3	2.9
PS	20	8.0	11.4	8.4	8.1	2.3	2.9
MO	20	7.8	9.3	-11.8	-11.3	2.1	2.7
PO	20	14.5	13.7	-23.7	-23.1	2.1	2.8
ES	120	3.7	5.4	0.3	0.3	1.4	1.8
PS	120	10.9	13.5	14.3	14.0	1.4	1.8
MO	120	19.1	18.3	-26.7	-26.6	0.2	0.4
PO	120	26.7	25.7	-38.6	-38.3	0.5	0.9

then apply the parametrized PER model to compute the predicted PER curves using the calculated SIR values, and compare them against the measured PER. Fig. 11(b) presents the resulting PER curves for different Wi-Fi 6E data rates. Overall, the PER predicted by our model using the Exhaustive Sweep method (dashed lines) shows strong similarity with the measured PER (solid lines), despite a visible offset in the curves' onset point. Tab. II reports a detailed breakdown of our model's performance in both *office* and *hallway* for different SCD estimation methods and UWB PSDU lengths. Our model parametrized with ES exhibits an average deviation of only 0.3 % in *office* and *hallway*, respectively, for large PSDUs; and of 4.7 % for short PSDUs.

VI. Discussion & Future Work

Our modeling approach represents a first step towards understanding UWB performance under Wi-Fi 6E interference. Several opportunities remain to refine and extend our model.

Dedicated parameters for different frame sections. The current model assumes uniform sensitivity across all sections of the UWB frame, and the estimated c and k parameters are tuned to represent the frame as a whole. To further improve the model's accuracy, future work could focus on estimating separate c and k parameters for each frame section.

Number of Wi-Fi stations. Our study focuses on Wi-Fi 6E traffic generated by a single station. Extending the model with the ability to capture the impact of traffic sent by multiple Wi-Fi stations on UWB performance is an important direction for future work. This entails: (i) modeling the change in traffic arising from Wi-Fi's channel access protocol, and (ii) capturing the effects of concurrent packet transmissions from multiple stations enabled by Wi-Fi 6E's OFDM capabilities.

UWB PHY settings and traffic profiles. This work studies how key Wi-Fi 6E PHY parameters affect UWB PER under interference, using periodic UWB traffic and varying only the UWB frame length. Extending this analysis to cover a broader range of UWB PHY settings and traffic patterns is a promising direction for future work that could further enhance the model.

Impact of Wi-Fi 7 traffic on UWB. The IEEE 802.11be standard (Wi-Fi 7), approved in late 2024, is currently the latest revision of Wi-Fi. Building on Wi-Fi 6E and operating in the same frequency bands, Wi-Fi 7 introduces key enhancements such as support for bandwidths up to 320 MHz and Multi-Link Operation (MLO), which enables simultaneous transmission and reception across multiple frequency bands and channels [25]. These features substantially increase maximum link rates beyond those of Wi-Fi 6E. As certification and commercialization of Wi-Fi 7 routers are still in the early stages, this paper focuses exclusively on results obtained with Wi-Fi 6E devices. However, our modeling approach is generic and readily extends to Wi-Fi 7, and we have confirmed this through preliminary tests with early Wi-Fi 7 hardware.

VII. Conclusion

We presented a methodological framework and model for predicting the PER of UWB communication under Wi-Fi 6E interference. In a first step, we recorded the UWB PER with different Wi-Fi 6E traffic profiles and PHY settings. Our analysis revealed that the Wi-Fi 6E channels' center frequency and bandwidth can account for an 11 dB difference in the UWB sensitivity; in contrast to the Wi-Fi 6E data rates and UWB payload length, whose impact is only up to 4.76 dB and 2.5 dB. Conversely, different Wi-Fi 6E data rates and UWB payload lengths significantly impact the maximum PER up to approximately 55%. We recorded traces of Wi-Fi 6E traffic and used them in combination with the previously-acquired PER to parametrize the proposed model. Our experimental evaluation demonstrated that our model can accurately predict the expected PER for a given Wi-Fi 6E traffic profile, with average deviations as low as 3.6% and 9.7% for conducted and wireless measurements, respectively.

Acknowledgments

This work has been supported by the BMK, BMAW, and FFG, Contract No. 881844: "Pro²Future" (Products and Production Systems of the Future), within the ENHANCE-UWB project.

References

[1] A. Ledergerber *et al.*, "A Robot Self-Localization System using One-Way Ultra-Wideband Communication," in *Proc. of the IROS Conf.*, 2015.
[2] S. Wang *et al.*, "UMusic: In-car Occupancy Sensing via High-resolution UWB Power Delay Profile," in *Proc. of the 23rd SenSys Conf.*, 2025.
[3] V. Di Pietra *et al.*, "A Low-Cost ICT Solution to Support Visitors in Touristic Caves," in *Proc. of the 12th MMT Symposium*, 2023.
[4] F. Hachem *et al.*, "Fine-Grained Stop-Move Detection with UWB: Quality Metrics and Real-World Evaluation," *ACM TOSN*, 2025.
[5] M. Charlier *et al.*, "Challenges in Using Time Slotted Channel Hopping with UWB Communications," in *Proc. of the 4th IoTDI Conf.*, 2019.
[6] M. Schuh *et al.*, "Understanding Concurrent Transmissions over Ultra-Wideband Complex Channels," in *Proc. of the 22nd SenSys Conf.*, 2024.
[7] H. Brunner *et al.*, "Understanding and Mitigating the Impact of Wi-Fi 6E Interference on Ultra-Wideband Communications and Ranging," in *Proc. of the 21st IPSN Conference*, 2022.
[8] M. Stocker *et al.*, "On the Performance of IEEE 802.15.4z-Compliant UWB Devices," in *Proc. of the 5th CPS-IoTBench Workshop*, 2022.
[9] M. Schuh *et al.*, "First Steps in Benchmarking the Performance of Heterogeneous Ultra-Wideband Platforms," in *Proc. of the 5th CPS-IoTBench Workshop*, 2022.
[10] FiRa Consortium, "Spectrum Position Statement," 2023. [Online]. Available: https://tinyurl.com/3fa5jbph
[11] C. Monka-Ewe *et al.*, "Coexistence of Mobile Broadband IMT Systems and UWB Keyless Entry Systems above 6.5 GHz," arXiv, Tech. Rep. 2401.17889, 2024. [Online]. Available: https://arxiv.org/abs/2401.17889
[12] Z. Ahmadian and L. Lampe, "Performance Analysis of the IEEE 802.15.4a UWB System," *IEEE Trans. on Comm.*, vol. 57, no. 5, 2009.
[13] O. Abedi and M. Yagoub, "Performance Comparison of UWB Pulse Modulation Schemes under White Gaussian Noise Channels," *International Journal of Microwave Science and Technology*, 2012.
[14] M. Hämäläinen *et al.*, "On the Performance Comparison of Different UWB Data Modulation Schemes in AWGN Channel in the Presence of Jamming," in *Proc. of the IEEE Radio and Wireless Conf.*, 2002.
[15] M. Hämäläinen and J. Iinatti, "Analysis of Interference on DS-UWB System in AWGN Channel," in *Proc. of the Ultra-Wideband Conf.*, 2005.
[16] S. Hechenberger *et al.*, "Performance Evaluation of Detection-based UWB Ranging in Presence of Interference," in *Proc. of the 55th Asilomar Conference on Signals, Systems, and Computers*, 2021.
[17] ——, "Low-Complexity Wideband Interference Mitigation for UWB ToA Estimation," *Sensors*, vol. 23, no. 13, 2023.
[18] ——, "Performance Bounds of UWB TOA Estimation in Presence of Wi-Fi 6E Wideband Interference," in *Proc. of the 14th IPIN Conf.*, 2024.
[19] S. J. Shellhammer, "Estimation of Packet Error Rate Caused by Interference using Analytic Techniques -– A Coexistence Assurance Methodology," IEEE, Tech. Rep. 802.19-05/0029r0, 2005.
[20] ——, "Probability of Bluetooth/WLAN Packet Collision," IEEE, Tech. Rep. 19-06-0021-00-0000, 2006.
[21] IEEE 802.15.4 Working Group, "IEEE Standard for Local and Metropolitan Area Networks – Part 802.15.4-2011: LR-WPANs," 2011.
[22] ——, "IEEE Standard for Low-Rate Wireless Networks – Part 802.15.4z-2020: Enhanced UWB PHYs and Ranging Techniques," 2020.
[23] B. Großwindhager *et al.*, "Enabling Runtime Adaptation of Physical Layer Settings for Dependable UWB Communications," in *Proc. of the 19th WoWMoM Symposium*, 2018.
[24] IEEE 802.11 Working Group, "IEEE Standard for Information Technology – Part 802.11-2020: Wireless LAN MAC and PHY Specs," 2021.
[25] C. Chen *et al.*, "Overview and Performance Evaluation of Wi-Fi 7," *IEEE Communications Standards Magazine*, vol. 6, no. 2, 2022.
[26] E. Khorov *et al.*, "A Tutorial on IEEE 802.11ax High Efficiency WLANs," *IEEE Comm. Surveys & Tutorials*, vol. 21, no. 1, 2019.
[27] M. S. Afaqui *et al.*, "IEEE 802.11ax: Challenges and Requirements for Future High Efficiency WiFi," *IEEE Wireless Comm.*, vol. 24, 2017.
[28] LitePoint Corporation, "A Guide to Wi-Fi 6E — Wi-Fi 6 in the 6 GHz Band," 2020. [Online]. Available: https://tinyurl.com/ywdduy2b
[29] J. Tiemann *et al.*, "Experimental Evaluation of IEEE 802.15.4z UWB Ranging Performance under Interference," *Sensors*, vol. 22, no. 4, 2022.
[30] G. Carfano *et al.*, "Impact of FR1 5G NR Jammers on UWB Indoor Position Location Systems," in *Proc. of the IPIN Conf.*, 2019.
[31] N. D. Lyholm *et al.*, "Evaluating the Impact of 5G NR Interference on Ultra-Wideband (UWB) Ranging Systems," Aalborg University, Tech. Rep., 2025. [Online]. Available: https://tinyurl.com/ajb2pj3y
[32] G. Cena *et al.*, "Evaluating and Modeling IEEE 802.15.4 TSCH Resilience against Wi-Fi Interference in New-Generation Highly-Dependable WSNs," *Ad Hoc Networks*, vol. 106, 2020.
[33] J. Huang *et al.*, "Beyond Co-existence: Exploiting WiFi White Space for Zigbee Performance Assurance," in *Proc. of the ICNP Conf.*, 2010.
[34] W. Yuan *et al.*, "A Coexistence Model of IEEE 802.15.4 and IEEE 802.11b/g," in *Proc. of the 14th SCVT Symposium*, 2007.
[35] C. A. Boano and K. Römer, "External Radio Interference," in *Radio Link Quality Estimation in Low-Power Wireless Networks*, ser. SpringerBriefs in Electrical and Computer Engineering - Cooperating Objects, 2013.
[36] A. Abdelfattah and N. Malouch, "Modeling and performance analysis of Wi-Fi networks coexisting with LTE-U," in *Proc. of the IEEE INFOCOM Conf.*, 2017.
[37] A.-k. Ajami and H. Artail, "On The Modeling and Analysis of Uplink and Downlink IEEE 802.11ax Wi-Fi With LTE in Unlicensed Spectrum," *IEEE Transactions on Wireless Communications*, vol. 16, no. 9, 2017.
[38] J. G. Proakis and M. Salehi, *Communication Systems Engineering*. Prentice-Hall, 2002, ch. 7.6 Probability of Error for Signal Detection in Additive White Gaussian Noise.
[39] R. H. Byrd *et al.*, "Approximate Solution of the Trust Region Problem by Minimization over Two-dimensional Subspaces," *Mathematical Programming*, vol. 40, 1988.
[40] A. F. Molisch *et al.*, "A Comprehensive Standardized Model for Ultra-wideband Propagation Channels," *IEEE Transactions on Antennas and Propagation*, vol. 54, no. 11, 2006.